

Demystify Transformers & Convolutions in Modern Image Deep Networks

Xiaowei Hu, Min Shi, Weiyun Wang, Sitong Wu, Linjie Xing, Wenhai Wang, Xizhou Zhu, Lewei Lu, Jie Zhou, Xiaogang Wang, Yu Qiao, and Jifeng Dai.

Abstract—Vision transformers have gained popularity recently, leading to the development of new vision backbones with improved features and consistent performance gains. However, these advancements are not solely attributable to novel feature transformation designs; certain benefits also arise from advanced network-level and block-level architectures. This paper aims to identify the real gains of popular convolution and attention operators through a detailed study. We find that the key difference among these feature transformation modules, such as attention or convolution, lies in their spatial feature aggregation approach, known as the “spatial token mixer” (STM). To facilitate an impartial comparison, we introduce a unified architecture to neutralize the impact of divergent network-level and block-level designs. Subsequently, various STMs are integrated into this unified framework for comprehensive comparative analysis. Our experiments on various tasks and an analysis of inductive bias show a significant performance boost due to advanced network-level and block-level designs, but performance differences persist among different STMs. Our detailed analysis also reveals various findings about different STMs, such as effective receptive fields and invariance tests. All models and codes used in this study are publicly available at <https://github.com/OpenGVLab/STM-Evaluation>.

Index Terms—Spatial token mixer, transformer, CNN, and image deep network.

arXiv:2211.05781v2 [cs.CV] 1 Dec 2023

1 INTRODUCTION

Vision transformers [1] have revolutionized the landscape of visual backbone models, inspiring a set of deep networks incorporating attention [2], [3], [4], convolution [5], [6], [7], and hybrid [8], [9] blocks. These networks consistently demonstrate performance gains attributed to novel feature transformation operators. However, it is essential to acknowledge the potential influence of advanced network engineering techniques, including macro architecture design [10] and training recipes [3], [5], [11]. This broader context prompts a critical question that *do the observed performance gains primarily stem from novel operator designs or from the adoption of advanced network engineering techniques?*

To address this inquiry, we conduct a comprehensive survey of recent vision backbones featuring novel operators [2], [3], [4], [5], [13]. Our examination reveals that the distinctions among these operators, and their asserted novelty, primarily hinge on the approach to spatial feature aggregation, commonly referred to as the Spatial Token Mixer (STM). Notably, our scrutiny aligns with the broader

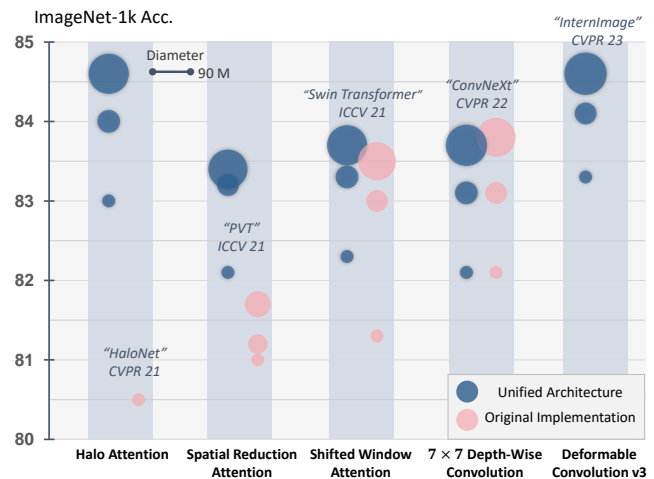


Fig. 1. Evolution of spatial token mixers. While consistent performance gains are observed using the original implementation or reported results, unifying network engineering techniques (overall architecture and training recipe) reveals that relatively early STMs, such as halo attention, achieve state-of-the-art performance.

- X. Hu, S. Wu, L. Xing, W. Wang, and Y. Qiao are with Shanghai Artificial Intelligence Laboratory.
- M. Shi is with Huazhong University of Science and Technology and Shanghai Artificial Intelligence Laboratory.
- W. Wang is with Shanghai Artificial Intelligence Laboratory and Fudan University.
- X. Zhu and L. Lu are with SenseTime Research.
- J. Zhou is with Tsinghua University.
- X. Wang is with the Chinese University of Hong Kong.
- J. Dai is with Tsinghua University and Shanghai Artificial Intelligence Laboratory.
- Xiaowei Hu, Min Shi, Weiyun Wang, and Sitong Wu are the joint first authors.
- Jifeng Dai is the corresponding author of this work (dai-jifeng@tsinghua.edu.cn).

interest in understanding the true efficacy of STMs. A recent study, MetaFormer [10], underscores the significance of transformer block design in overall performance. Remarkably, MetaFormer demonstrates that the STM within the transformer block, specifically the attention layer, can be substituted with a simple mixing operation, such as pooling, without a substantial drop in performance. This finding serves as an additional motivation for our investigation into the authentic performance gains associated with various STMs, aiming to discover any potential biases arising from disparate network engineering practices.

To achieve this, we first construct a modern and unified

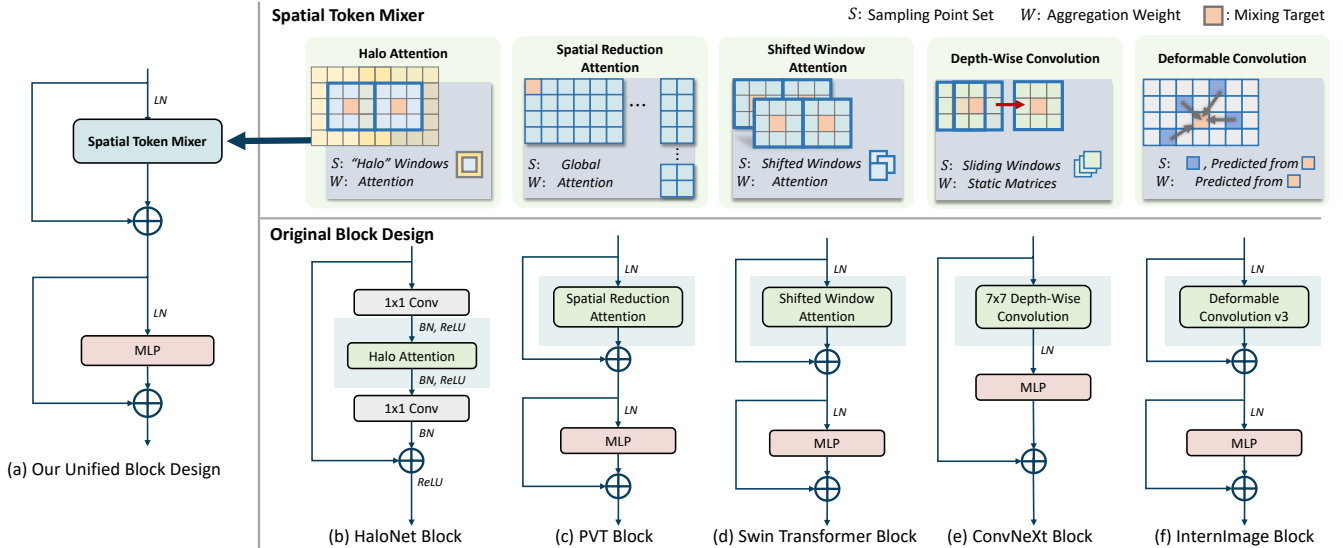


Fig. 2. The schematic illustration depicts (a) our unified block design (following the vanilla Transformer [12] block design) and spatial token mixer designs (top), along with the original block designs (bottom) of (b) HaloNet, (c) PVT, (d) Swin Transformer, (e) ConvNeXt, and (f) InternImage.

architecture for comparison, where we sequentially determine the stage-level design (*i.e.*, stem and transition layers) and block-level design (*i.e.*, the topology of basic blocks) by a series of experiments and analyses. We find that some macro designs such as different downsampling operations may affect the performances for a certain type of STM, and the proper block design can also contribute to performance gain significantly. We combine the findings and beneficial designs into a unified architecture. By instantiating different STMs on this architecture, we achieve comparable or even better results than the reported performance in their original papers, as shown in Fig. 1. Our study includes four pivotal STMs representing diverse approaches in vision backbones: local attention [2], [3], global attention [4], depth-wise convolution [5], and dynamic convolution [14]. Refer to Fig. 2 for a visual overview of these operations. Each STM is selected for distinct characteristics, ensuring a thorough exploration of spatial feature aggregation in the unified architecture.

Employing the instantiated models, we conduct an investigation and comparison of STMs across multiple dimensions. Initially, we assess the performance of different models on both upstream (classification) and downstream (object detection) tasks, using ImageNet-1k [15] and COCO [16] datasets. Our findings, as illustrated in Fig. 1, reveal performance gaps among various STMs, deviating from reported trends with original implementations. Notably, earlier STMs, imbued with advanced design principles, achieve comparable or superior performance compared to recent counterparts in both upstream and downstream tasks. Furthermore, STMs exhibiting vision-specific inductive bias and dynamic information modeling mechanisms, such as local attention and dynamic convolution, demonstrate relatively robust performance. Static convolution proves effective in low-capacity models (around 4.5M parameters) but lags behind larger-scale models. Additionally, we observe that the inter-window information transfer in local-attention STMs significantly influences performance.

Moreover, our aim extends beyond performance com-

parison to uncover distinctive characteristics in different STMs. The design of an STM, reflecting prior knowledge and constraints in the hypothesis space (inductive bias), is analyzed for its impact on learned model characteristics, including locality, shift, rotation, and scale invariance. Observations reveal significant variations among STMs in capturing information during feature aggregation, termed as the effective receptive field (ERF) [17]. Further exploration highlights that a larger ERF does not guarantee improved performances, and the benefits may saturate as the model scales up. In our invariance test, models exhibiting superior performance also demonstrate heightened robustness against variations, suggesting the learnability of invariance through data and diverse augmentations. Additionally, static convolution, employing weight-sharing and emphasizing locality, demonstrates more pronounced translation invariance. Notably, leveraging a flexible sampling strategy for dynamic aggregation, dynamic convolution (DCNv3 [14]) outperforms other STMs in rotation and scaling invariance.

Our contributions can be summarized as follows:

- We experimentally compare typical spatial token mixers, unveiling the characteristics of local attention, global attention, depth-wise convolution, and dynamic convolution.
- Distilling effective network engineering techniques from modern backbone designs, we create a unified architecture that enhances spatial token mixer performance compared to their original implementations.
- Our experiments using the unified architecture on image classification and object detection tasks reveal significant performance improvements due to network engineering techniques. Despite this, performance gaps persist among different STMs, with the earlier halo attention achieving state-of-the-art results.
- Analyzing the impact of inductive bias on STM characteristics, we challenge the notion that the effective receptive field alone is a metric for evaluating STM quality. Our findings underscore that STMs with strong

TABLE 1
Comparison of various spatial token mixer designs.

STM	Type	Abbr.	Sampling Point Set	Aggregation Weight	Method
Halo Attention	Local Attention	Halo-Attn	Local	Dynamic	HaloNet [2]
Spatial Reduction Attention	Global Attention	SR-Attn	Global	Dynamic	PVT [18]
Shifted Window (Swin) Attention	Local Attention	SW-Attn	Local	Dynamic	Swin Transformer [3]
Depth-Wise Convolution	Convolution	DW-Conv	Local	Static	ConvNeXt [5], DWNet [19]
Deformable Convolution v3	Dynamic Convolution	DCNv3	Global	Dynamic	InternImage [14]

performance exhibit high invariance, emphasizing the role of STM design in contributing to this invariance.

2 RELATED WORK

2.1 Convolution-Based Spatial Token Mixers

Leveraging image-specific priors, such as sparse interactions, parameter sharing, and translation equivalence [20], convolution has earlier occupied vision backbones [21], [22], [23]. The evolution of vision backbones primarily centered on architectural aspects, including residual learning [24], dense connections [25], grouping techniques [26], [27], and channel attention [28]. In contrast, spatial feature aggregation mechanisms received less attention. Approaches like deformable convolution [29] and non-local methods [30] introduced flexible point sampling and long-range dependency, breaking the locality constraint. With the emergence of vision transformers [1], convolution has adapted to more advanced network engineering designs [5], [6], [7]. Notably, Han *et al.* [19] demonstrated that introducing dynamic weight computation into depth-wise convolution can achieve comparable or slightly superior performance compared to local vision transformers.

2.2 Attention-Based Spatial Token Mixers

Since the introduction of the transformer into vision [1], its core operator, attention, has significantly challenged the dominance of convolution. Unlike standard convolution, attention boasts a global receptive field and dynamic spatial aggregation. However, the dense attention calculation comes with a substantial computational overhead, scaling quadratically with the size of input maps. This becomes particularly impractical for applying vanilla attention to feature pyramids, especially on large feature maps. Consequently, attention operators in vision typically reduce the number of locations attended during attention calculation. Approaches like PVT [4], [18] and Linformer [31] employ global attention on down-sampled feature maps, while Pale Transformer [32] uses pale operation to sample features across the entire feature map. Drawing inspiration from the locality prior of convolution, local attention is introduced [2], [3], where attention is constrained within local windows. Since these local windows are non-overlapping, mechanisms for inter-window information transfer, such as “haloing” [2] and shifted windows [3], have been developed.

2.3 Optimizing Engineering and Backbone Evaluation

Instead of introducing novel spatial token mixers, some research focuses on identifying advantageous network engineering techniques. ResNet-RSB [33] demonstrates that an

advanced training recipe can significantly enhance performance compared to a naïve setting. ConvNeXt [5] modernizes a standard ResNet by incorporating recent advancements in both training recipes and network architecture design. MetaFormer [10] underscores the significant role of the abstracted architecture of the Transformer block in achieving competitive performance. Recent work by Yu *et al.* [34] further validates the effectiveness of Transformer-style block design, achieving impressive performance using basic or common mixers. Despite MetaFormer’s emphasis on the importance of the transformer block, diverting attention from STMs, we observe performance gaps among different STMs. Toolkit initiatives like Timm [35] offer off-the-shelf or reproduced models but lack a comprehensive comparison of different STMs under a unified architecture. As depicted in Fig. 1, an advanced STM design, such as halo-attention, coupled with a modern network architecture, outperforms other STMs with the same architecture by a significant margin. Additionally, we find that network engineering techniques extend beyond block-level design. We conduct more ablation studies on stage-level design and compare them with ConvNeXt’s block design. It’s important to note that our primary goal is not to construct an extremely optimized framework but to comprehensively compare and analyze different STMs under a unified setting from various perspectives.

3 SPATIAL TOKEN MIXER

3.1 Definition of Spatial Token Mixer

The Spatial Token Mixer (STM) aims to aggregate spatial features around each pixel to transfer contextual information. Given an input feature map $\mathbf{X} \in \mathbb{R}^{C \times H \times W}$, we define the token mixing function \mathcal{M} for the mixing target point p as:

$$\mathcal{M}(p) = W_o \sum_{k \in S} w_{pk} \cdot \mathbf{X}(k), \quad (1)$$

where S denotes the *sampling point set* that records the pixels to attend; w_{pk} denotes the aggregation weight with respect to the sample point p ; and W_o is the output projection matrix. In practice, STMs typically employ a multi-head strategy, projecting or splitting the input feature into different heads.

STMs vary in the generation of the sampling point set and the aggregation weight, as summarized in Table 1. In this study, we consider four prevalent types of STMs for comparison: depth-wise convolution, dynamic convolution, local attention, and global attention.

3.2 Taxonomy of Spatial Token Mixer

3.2.1 Depth-Wise Convolution

Depth-wise convolution aggregates features in an input-independent manner. The sampling point set consists of sliding windows centered at the mixing target point p , and the aggregation weight is represented by a learnable weight matrix—the convolution kernel. Despite its simplicity, recent convolution networks [5], [6] have demonstrated that depth-wise convolution, when combined with advanced architecture and training recipes, can achieve comparable performance to top-performing vision transformers. In our comparison, we employ a 7×7 depth-wise convolution, following the configuration of DWNNet [19] and ConvNeXt [5]. Specifically, we incorporate input and output projection layers before and after the depth-wise convolution in our unified block design.

3.2.2 Dynamic Convolution

Dynamic convolution is input-dependent, where both the sampling point set and aggregation weights are generated conditioned on the inputs. For instance, the widely-used deformable convolution [14], [29], [36] infers per-pixel sampling point sets and aggregation weights from input features for spatial aggregation. In this comparison, we utilize deformable convolution v3 (DCNv3) from InternImage [14] as the representative example of dynamic convolution. We employ nine sampling points, consistent with the original implementation. The offsets and weights for these sampling points are determined through a 3×3 depth-wise convolution followed by a linear projection. Weights are normalized using a `Softmax` function.

3.2.3 Global Attention

Global attention-based STM mixes features across the entire spatial domain, with aggregation weights dynamically generated through the inner product between the target point and each sampling point. While global attention offers a theoretically global receptive field without introducing image-specific inductive bias like locality, it comes with a significant computational overhead that scales quadratically with input resolutions. To integrate global attention STMs into pyramid-like vision backbones, optimization for efficiency is essential. A common practice involves constraining the cardinality of the sampling point set [4], [13], [32]. In our experiments, we adopt spatial reduction attention from PVT [4]. During attention computation, the *key* and *value* feature maps are downsampled.

3.2.4 Local Attention

An alternative approach to optimizing global attention involves introducing locality, i.e., restricting the sampling point set to local windows [2], [3], rather than the entire spatial domain. Given the intricacy of attention, local attention, in contrast to the densely overlapped sliding windows in convolution, employs non-overlapping local windows where pixels within each window share the same sampling point set. To facilitate information transfer among different windows, HaloNet [2] enlarges each window with an additional band resembling a “halo.” Swin Transformer [3]

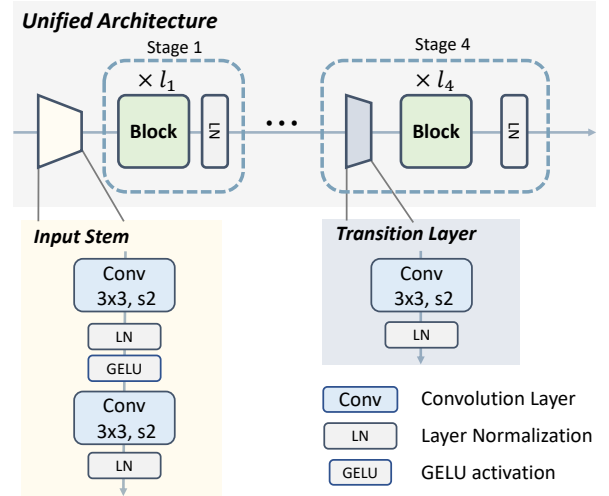


Fig. 3. Unified architecture design. Overlapped downsampling is applied to the input stem and transition layer, while the standard transformer [12] block design is adopted.

introduces shifted windows to create overlapping sampling points, enabling information transfer between different blocks. For a comprehensive exploration of the design principles of local attention STMs, we include both halo attention from HaloNet and shifted window attention from Swin Transformer in our comparison.

4 UNIFIED ARCHITECTURE AND TRAINING RECIPE

This section presents our unified architecture and training strategies. We systematically analyze the stage-level and block-level architecture design through sequential ablations. Subsequently, we instantiate different STMs discussed in Sec. 3 into the unified architecture for comprehensive comparison.

4.1 Stage-Level Design

First, we determine the stage-level design of the unified architecture, focusing on the input stem and transition layers. Recent backbones [3], [4], [5] often perform downsampling in the transition layer, with downsampling categorized into overlapped [10] (a 3×3 convolution with a stride of two) and non-overlapped [3], [5] (a 2×2 convolution with a stride of two) patch merging. Here, we compare the performance of these two downsampling methods.

As depicted in Table 2 (left part), the use of overlapped downsampling improves the classification accuracy of Swin-Transformer by 1.2%, while the improvement for ConvNeXt is marginal (0.1%). A plausible explanation is that overlapped downsampling facilitates information transfer among windows for local attention STMs, which complements the inherent weakness of non-overlapped window partition: the lack of inter-window information transfer. However, for the 7×7 depth-wise convolution used in ConvNeXt, minor gains are observed, as the sliding windows of convolution are densely overlapped. Hence, we adopt the 3×3 convolutions with a stride of two for the input stem and transition layers; refer to Fig. 3 for details.

TABLE 2
The ablation study on block and stage design.

	Stage Design		Block Design		
	STM	Original	Unified	STM	Original
SW-Attn	81.1	82.3	Halo-Attn	80.5	83.0
DW-Conv	82.1	82.2	DW-Conv	82.2	82.2

4.2 Block-Level Design

Block-level design determines the topology of operators, specifying their positions and connections. Before the emergence of vision transformers, most vision models adhere to the block design of standard ResNet [24], featuring a single skip connection with standard convolution (see the HaloNet block design in Fig.2). The transformer block [1], [12] introduces a distinct approach by segregating STM and channel feature transformation into two residual connections, each with a normalization layer (refer to the unified block design in Fig.2). Metaformer [10] demonstrates that the transformer-style block design itself significantly contributes to the performance gain of vision transformers.

Hence, for the unified architecture, we adopt a standard transformer block as depicted in Fig. 2 and replace the attention with different types of STMs. In the right part of Table 2, the unified block design substantially enhances the performance of HaloNet (+2.5%), which employs the ResNet-style block design in its original implementation. However, ConvNeXt [5] achieves comparable performance with depth-wise convolution using an improved ResNet block design (denoted as “original” in Table 2). This suggests that the transformer’s block design may not necessarily be a universal rule. Despite this, for the sake of uniformity in architecture for comparison, we continue to use the unified block design for all compared STMs, including depth-wise convolution. We further compare the compatibility of the ConvNeXt block and the transformer block for different STMs in Sec. 5.3. Here, we denote the overall network, where the depth-wise convolution used in the unified architecture, as “U-DWConv”.

4.3 Model Configuration and Training Strategies

4.3.1 Model Configuration

To facilitate a comprehensive comparison, we instantiate STMs on models with four different scales: micro ($\sim 4.5M$), tiny ($\sim 30M$), small ($\sim 50M$), and base ($\sim 90M$). Implementations under our unified architecture are denoted with the prefix “U-”. Parameters and MACs of different models are detailed in Table 4. It is worth noting that micro models, with only around 4.5M parameters, are seldom discussed for standard backbones. Given the differing complexities of various STMs, the blocks per stage and channel numbers also vary. Further details can be found in the supplementary material.

4.3.2 Image Classification

We consolidate training techniques from recent top-performing networks [3], [5] into a unified strategy. Models undergo 300 training epochs on ImageNet-1k [15] with the AdamW optimizer [37]. Training specifics include gradient clipping with a maximum norm of 5.0, weight decay of

TABLE 3
ImageNet-1k classification training settings.

Training Configurations	Convolutions	Transformers
training epochs	300	300
batch size	4096	1024
warm-up epochs	20	20
learning rate schedule	cosine decay	cosine decay
base learning rate	4e-3	1e-3
optimizer	AdamW	AdamW
gradient clip	5	5
weight decay	0.05	0.05
layer scale	1e-6	1e-6
label smoothing	0.1	0.1
EMA decay	0.9999	0.9999
input resolution	224 × 224	224 × 224
mixup	0.8	0.8
cutmix	1.0	1.0
random erasing	0.25	0.25
color jitter	0.4	0.4
test crop ratio	0.875	0.875

0.05, layer scale [38] starting at 10^{-6} , label smoothing [39] at 0.1, and stochastic depth [40]. Standard data augmentation practices [3], [5] are employed, incorporating RandAugment [41], Mixup [42], Cutmix [43], Random Erasing [44], and color jitter. Training settings are uniform across all models, except for batch size and drop path rate. Batch sizes are set to 1,024 for U-Swin Transformer, U-HaloNet, and U-PVT, and 4,096 for U-DWConv and U-InterImage, as larger batch sizes favor convolutional STMs. Drop path rates adhere to the original settings in their respective papers. The learning rate is determined as $(\text{batch size}/1024) \times 10^{-3}$ with a linear warm-up lasting 20 epochs and cosine decay. Refer to Table 3 for detailed parameters.

4.3.3 Object Detection

We employ object detection as the downstream task and integrate the models into Mask-RCNN [45] for evaluation. Models are trained and evaluated on COCO `train2017` and `val2017` with single-scale training and evaluation. Images are resized so that the shorter sides equal 800 pixels while the longer sides do not exceed 1,333 pixels. All models are trained using AdamW [37] for 12 epochs with a batch size of 16. The learning rate is set to 10^{-4} and drops by $10\times$ at the eighth and tenth epochs. The weight decay is set to 0.05 and the warmup iterations are 1000. Drop path rates are set to 0.1, 0.2, 0.2, and 0.3 for micro, tiny, small, and base models, respectively.

5 RESULTS AND DISCUSSION

5.1 Image Classification

We present the comparison of different STMs on ImageNet-1k classification in Table 4. U-InterImage achieves the best performance on tiny and small models but slightly falls behind U-HaloNet on micro and base scales. Halo-Attn demonstrates comparable performance with DCNv3 and outperforms SW-Attn in Swin Transformer significantly. This suggests that “haloing” is a practical window information transfer design for local-attention STMs when performance is a priority. It highlights that the relatively early STM, such as halo attention, can yield a significant

TABLE 4

Classification accuracy on ImageNet-1k. “U-” denotes that the models are re-implemented in our unified architecture.

Scale	Method	#Params	FLOPs	ImageNet-1k Acc
Micro	U-HaloNet	4.4M	0.65G	75.8%
	U-PVT	4.3M	0.57G	72.8%
	U-Swin Transformer	4.4M	0.71G	74.4%
	U-DWConv	4.4M	0.65G	75.1%
	U-InternImage	4.3M	0.65G	75.3%
Tiny	U-HaloNet	31.5M	4.75G	83.0%
	U-PVT	30.8M	4.56G	82.1%
	U-Swin Transformer	31.5M	4.91G	82.3%
	U-DWConv	31.9M	5.01G	82.2%
	U-InternImage	29.9M	4.83G	83.3%
Small	U-HaloNet	52.8M	8.92G	84.0%
	U-PVT	50.5M	7.33G	83.2%
	U-Swin Transformer	52.9M	9.18G	83.3%
	U-DWConv	54.4M	9.40G	83.1%
	U-InternImage	50.1M	8.24G	84.1%
Base	U-HaloNet	93.3M	15.84G	84.6%
	U-PVT	91.1M	12.73G	83.4%
	U-Swin Transformer	93.4M	16.18G	83.7%
	U-DWConv	95.8M	16.64G	83.7%
	U-InternImage	97.5M	16.08G	84.5%

performance gain with advanced network engineering techniques. Using the 7×7 DW-Conv can achieve comparable performance with SW-Attn and surpasses SW-Attn on micro models. U-PVT with global attention (SR-Attn) as STM shows obvious disadvantages under micro models but quickly becomes comparable with U-Swin Transformer on other scales.

5.2 Object Detection

We use object detection as the down-stream task to evaluate different STMs. Table 5 reports the detection results, where (i) STMs with high accuracy (Halo-Attn and DCNv3) retain the advantages on object detection and surpass the other STMs by large margins; (ii) global attention (U-PVT) performs the worst on micro models but becomes on par with SW-Attn on other scales; (iii) depth-wise convolution shows strong performance among the micro models, but is not competitive at larger scales. In our experiments, both local-attention- and convolution-based STMs with locality inductive bias perform better compared with the model using global spatial reduction attention.

5.3 Ablation Study of the Unified Architecture

In this section, we conduct an ablation study on the unified architecture design for STMs. As discussed in Sec.4.2, the 7×7 depth-wise convolution (DW-Conv) with the unified block design or ConvNeXt [5] block design yields similar performance. This raises the question of whether ConvNeXt’s block design can be an alternative to the transformer block design. Hence, we perform an ablation study for comparison, gradually transforming our unified architecture (A) into the ConvNeXt architecture (E).

As shown in Fig. 4, for the stage-level design, B shifts the layer normalization (LN) after the global average pooling in the decoder head based on A, and C removes LN after each stage based on B. For the block-level design, D adopts the block design of ConvNeXt (Fig.2(e)) based on A. Note that we keep our stem and transition layer (Fig.3) in all models.

TABLE 5

Object detection results on COCO.

Scale	Method	Box				Mask			
		AP	AP_s	AP_m	AP_l	AP	AP_s	AP_m	AP_l
Micro	U-HaloNet	40.3	24.5	43.0	53.7	37.3	18.7	39.7	55.2
	U-PVT	35.9	21.2	38.4	47.2	34.2	16.8	36.1	50.2
	U-Swin Transformer	36.6	22.3	39.1	48.0	34.6	17.2	36.7	50.1
	U-DWConv	39.2	23.0	42.6	51.0	36.4	17.8	39.2	52.7
	U-InternImage	39.5	22.8	42.9	52.7	36.6	17.4	39.4	53.6
Tiny	U-HaloNet	46.9	30.0	50.2	61.4	42.4	22.6	45.3	60.9
	U-PVT	44.2	27.5	47.4	59.1	40.6	21.1	43.4	59.5
	U-Swin Transformer	44.3	28.0	47.5	57.8	40.5	21.6	43.0	58.2
	U-DWConv	44.3	27.8	48.0	57.5	40.5	20.7	43.9	58.6
	U-InternImage	47.2	30.4	51.3	61.3	42.5	23.3	45.9	60.9
Small	U-HaloNet	48.2	31.2	52.5	63.2	43.3	23.4	47.0	62.3
	U-PVT	46.1	28.8	49.3	61.2	41.9	21.9	44.6	61.2
	U-Swin Transformer	46.4	28.2	50.0	61.5	42.1	21.8	45.2	60.7
	U-DWConv	45.6	28.5	49.8	59.8	41.2	21.9	44.7	59.4
	U-InternImage	47.8	30.3	51.8	62.4	43.0	23.1	46.3	61.7
Base	U-HaloNet	49.0	31.8	53.0	63.7	43.8	24.4	47.0	62.8
	U-PVT	46.4	29.0	49.8	62.2	42.3	22.3	45.1	61.8
	U-Swin Transformer	47.0	30.8	50.6	62.2	42.2	23.5	45.1	61.7
	U-DWConv	46.7	30.2	50.3	61.4	42.2	22.8	45.1	60.7
	U-InternImage	48.7	33.1	52.5	63.4	43.8	25.0	46.9	62.3

TABLE 6

Ablation study of the unified network architecture. Experiments are conducted on small-level models. We gradually modify our unified architecture (denoted by A) into the architecture of ConvNeXt (denoted by E). “Original” results are the reported results in their papers.

STM	A	B	C	D	E	Original
Halo-Attn	84.0	84.3	84.4	83.8	83.8	--
SR-Attn	83.2	83.4	83.4	78.6	79.4	81.7
SW-Attn	83.3	83.5	83.7	82.8	82.9	83.0
DW-Conv	83.1	83.1	83.3	83.2	83.6	83.1
DCNv3	84.1	84.1	84.0	83.8	83.6	--

The results in Table 6 reveal that: (i) for most STMs, adding LN after global average pooling (B) and removing stage normalization (C) consistently improve performance; (ii) except for DW-Conv, applying other STMs to the ConvNeXt-style block degrades performance (A and D). In contrast, DW-Conv shows a performance gain with the ConvNeXt-style block design. However, for a fair comparison, we retain the transformer-style block design. We keep the stage normalization, as additional normalization helps stabilize the training process as the model scales up [14], [46], a topic to be investigated in our future work.

5.4 Ablation Study of Local Attention

Local attention has gained popularity as a STM for vision models due to its notable performance and efficiency. However, our study reveals a significant performance gap among different implementations of local attention, such as Halo-Attn [2] and Swin-Attn [3]. This observation motivates us to conduct an in-depth analysis to identify the core factors affecting performance.

The main differences between Halo-Attn and Swin-Attn can be attributed to three factors: (i) Halo-Attn conducts inter-window feature transfer once every block, more frequently than Swin-Attn; (ii) Halo-Attn employs a larger window (sampling point set) with the extra “halo”; (iii) Halo-Attn shows a relatively isotropic feature aggregation

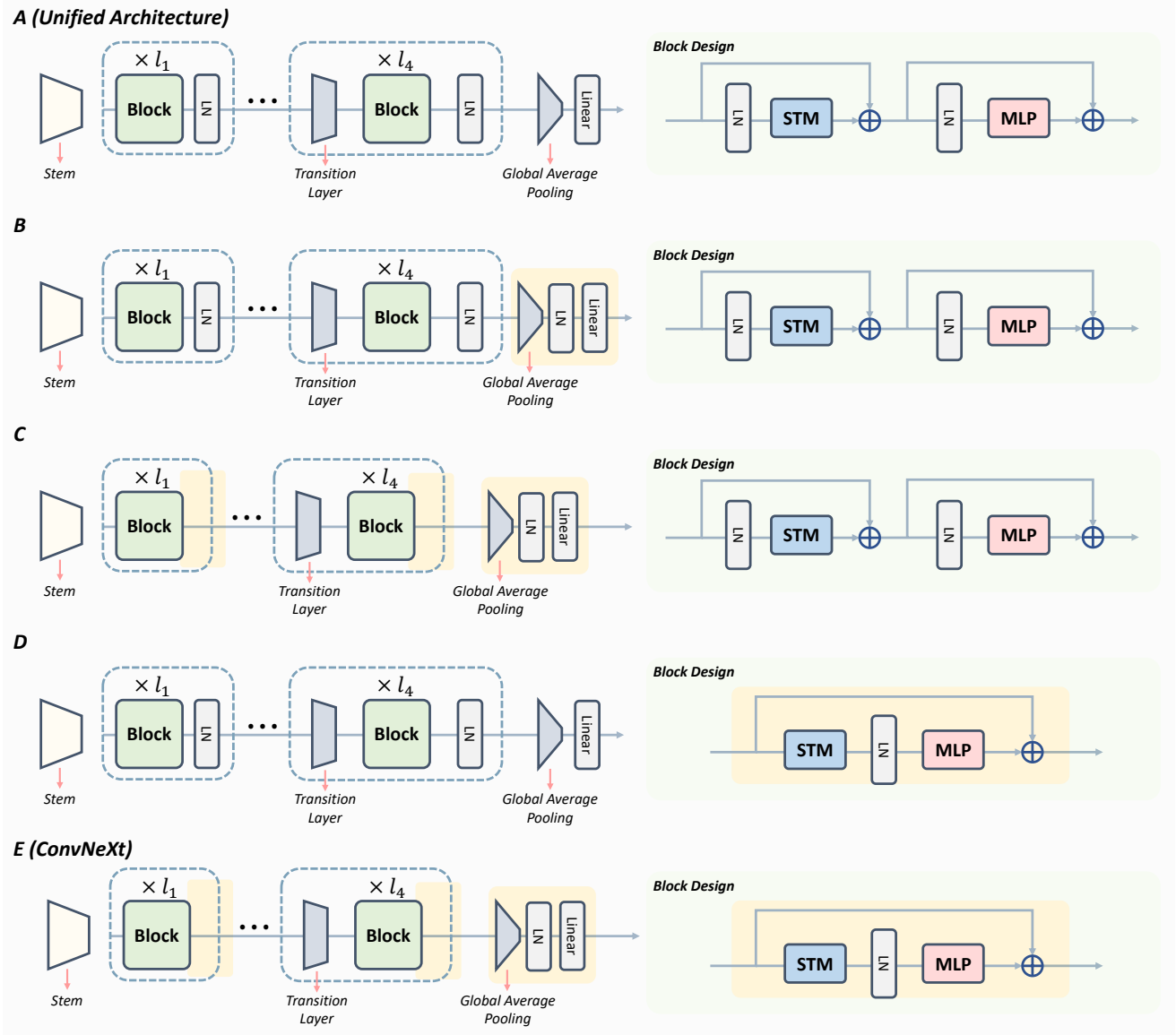


Fig. 4. The illustration showcases five architectures, transitioning from our unified architecture (A) to the ConvNeXt architecture (E). The yellow shadings in architectures B-E emphasize their differences compared with architecture A.

TABLE 7
Ablation study on local attentions in small models.

Methods	MACs	ImageNet-1k Acc
U-Swin Transformer	9.16	83.3
U-HaloNet	9.75	84.0
U-HaloNet-Switch	9.45	83.9
U-HaloNet-1px	9.32	83.8
U-HaloNet-Shift	9.75	82.7

pattern, while Swin-Attn tends to aggregate information from a particular direction (see Fig. 6). To investigate the impact of these factors, we introduce three new variants for Halo-Attn, as shown in Table 7. First, U-HaloNet-Switch is added, conducting inter-window information transfer every two blocks. Next, we introduce U-HaloNet-1px, with a halo size set to one. Finally, we shift the query window of Halo-Attn to the top-left corner while keeping the total window size unchanged to examine the effect of non-central

aggregation.

Our experimental results, presented in Table 7, demonstrate that the impact of window size and inter-window transfer frequency is not significant: halving the inter-window transfer frequency reduces MACs by 0.30G while still preserving performance, and reducing the halo size to one only results in a 0.2% accuracy drop. However, U-HaloNet-Shift shows a significant performance drop of 1.3% on accuracy, suggesting that the geometry of inter-window interaction is the crucial factor for local attention operators.

6 INDUCTIVE BIAS AND INVARIANT ANALYSIS

In this section, we explore the impact of the inductive bias of various STMs on learned model characteristics. We conduct analyses on effective receptive fields, translation invariance, rotation invariance, and scaling invariance.

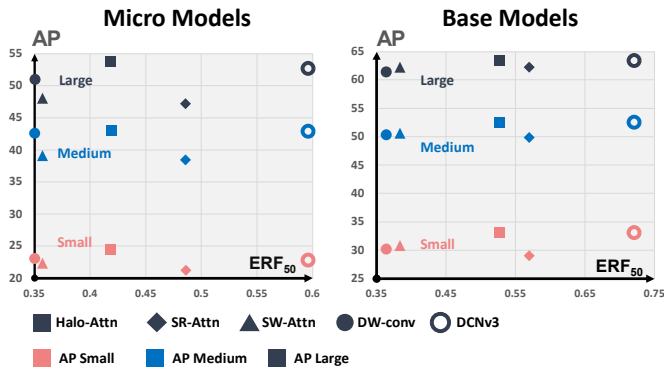


Fig. 5. The correlation between detection accuracy and effective receptive field. We depict the box Average Precision (box AP) for small, medium, and large objects on the COCO validation set in relation to the ERF@50 of micro and base models.

6.1 Effective Receptive Field

The effective receptive field (ERF) [17] of a unit in vision backbones refers to the region where the pixels influence the output of this unit. While the inductive bias introduced by different STMs sets the theoretical upper limit for the receptive field, the actual ERFs can vary. We employ the ERF toolbox [17] to assess the ERF of the center pixel in feature maps across different stages. Models trained on ImageNet-1k are used to compute the ERF maps. The ERF toolbox provides a gradient norm map, with each value indicating the impact of specific locations on the center point. By placing a gradually expanding window at the center, we determine the square length-to-input size ratio when the sum of the gradient norm within the window reaches 50% of the image size. This ratio, denoted as ERF@50, serves as the quantitative metric following [6].

We explore the relationship between Effective Receptive Field (ERF) and downstream performance in object detection. In Fig. 5, we present the box accuracy for small, medium, and large objects. Interestingly, we observe no strong correlation between ERF and detection accuracy. For instance, U-HaloNet exhibits comparable detection accuracy with smaller ERFs compared to U-InternImage. In the case of base models, accuracy comparisons across different scales remain consistent, and performance appears uncorrelated with ERF sizes. Therefore, we posit that ERF should not serve as a definitive metric for evaluating STM quality. A smaller ERF does not necessarily imply inferiority compared to STMs with larger ERFs.

Furthermore, our observations indicate that the design of STMs influences the shape of the effective receptive field. Fig. 6 showcases visualized ERFs of SW-Attn and Halo-Attn. Notably, the shifted windows in the ERF of Swin-Attn are evident, with more features aggregated from the bottom-right corner, aligning with the direction of the shifted window. Conversely, halo attention exhibits a more symmetrical ERF due to the “halo” window information transfer. Additional results and visualizations of ERFs can be found in the supplementary material.

6.2 Invariance Analysis

In this subsection, we assess the robustness of different STMs under various geometric transformations. We specif-

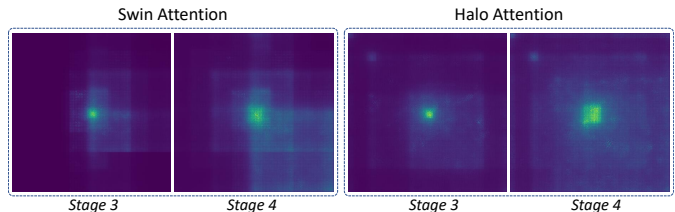


Fig. 6. The design of the spatial token mixer influences the shape of the ERF. We visualize the ERF maps at the last two stages of U-Swin Transformer and U-HaloNet. The asymmetric ERF of Swin attention is evident, showcasing the presence of shifted windows.

ically consider translation, rotation, and scaling for our analysis. Invariance can be inherent in the STM design, learned from training samples, or acquired through data augmentation. Convolution-based STMs inherently possess translation equivalence due to locality and weight sharing [20], while local-attention STMs maintain window-level translation equivalence. The translation equivalence closely relates to translation invariance, given that the feature map undergoes average pooling before entering the classifier in our case. Neither convolution-based nor attention-based STMs inherently incorporate inductive biases related to rotation or scaling.

6.2.1 Translation Invariance

Translation invariance refers to the model’s ability to maintain consistent outputs when input images undergo translation. We assess translation invariance in the classification task by introducing jitter to the images, ranging from 0 to 64 pixels. Following [47], we measure invariance by the probability that the model predicts the same label for the same input images when translated.

In the first row of Fig. 7, we observe the translation invariance of different STMs, noting that: (i) Convolution-based STMs (DCNv3 and depth-wise convolution) exhibit better translation invariance (see the first row in Fig. 7 (a)). (ii) U-PVT, utilizing global attention, performs the poorest in terms of translation invariance, likely due to the absence of translation equivalence. (iii) DCNv3 and halo attention consistently achieve the best performance even with translated images (see the first row in Fig. 7 (b)). (iv) Halo attention, depth-wise convolution, and DCNv3 demonstrate superior translation invariance initially, with DCNv3 improving its invariance during training (see the first row in Fig. 7 (c)).

6.2.2 Rotation Invariance

We evaluate rotation invariance on the classification task by rotating the images from 0° to 45° with a step of 5° . Similar to translation invariance, we measure prediction consistency under different rotation angles to assess the rotation invariance of different STMs.

From the second row in Fig. 7, we observe that: (i) DCNv3, with its input-dependent sampling strategy, exhibits strong robustness against rotation. (ii) Other STMs show comparable performance, with halo attention performing slightly better at larger rotation angles ($> 30^\circ$). (iii) Rotation invariance is comparable among all STMs at the beginning of the training process, except for Halo-Attn, which demonstrates superior rotation invariance. However,

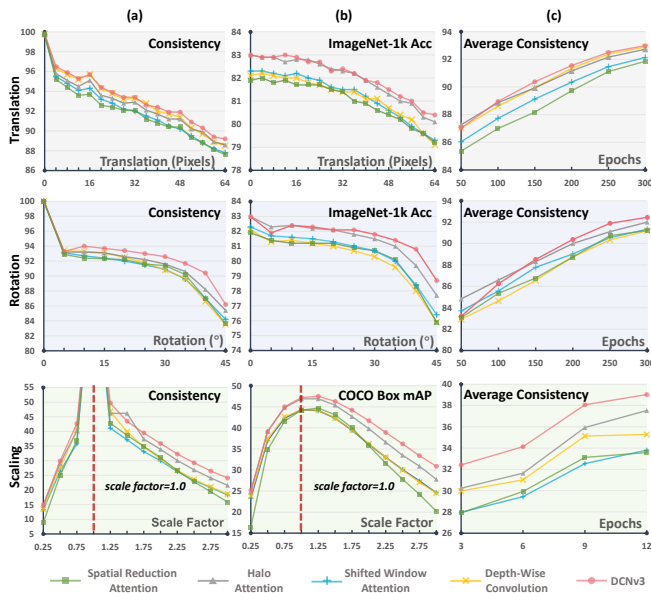


Fig. 7. Translation, rotation, and scaling invariance of STMs. (a) Prediction consistency. (b) Classification (detection) accuracy under input translation, rotation, and scaling. (c) Average prediction consistency at different training epochs.

DCNv3 quickly learns strong rotation invariance from the training data.

6.2.3 Scaling Invariance

Scaling invariance is assessed in object detection by scaling input images with factors from 0.25 to 3.0 in steps of 0.25. Box consistency serves as the invariance metric, where predicted boxes on scaled images are reverted to the original resolutions. Subsequently, the boxes predicted at the original resolutions are employed as ground truth boxes to compute the box mAP.

From the third row in Fig. 7, we observe that: (i) All STMs are sensitive to downscaling and exhibit comparable invariance with the input in small sizes. (ii) DCNv3 performs better when upscaling the image, with both the box consistency and box mAPs outperforming the others. (iii) Halo-Attn shows comparable invariance with depth-wise convolution in the early training stage but learns better invariance in the last three epochs.

6.2.4 Summary

Considering the results from translation, rotation, and scale invariance, we can conclude that STMs with strong performance exhibit relatively high invariance. However, the design of STMs also contributes to invariance; for example, depth-wise convolution attains comparable translation invariance with Halo-Attn. Moreover, DCNv3, which learns to generate the sampling point set conditioned on inputs adaptively, achieves the best invariance among all the STMs. This suggests the generalization and robustness of DCNv3 compared to other STMs with fixed sampling sets.

7 CONCLUSION AND LIMITATIONS

In this study, we conducted a comparison of popular Spatial Token Mixers (STMs) within vision backbones, establishing

a unified setting to isolate the impact of network engineering techniques. Through the distillation of successful network engineering strategies and the creation of a unified architecture via ablation studies, we integrate five representative STMs for thorough comparison. A series of experiments encompassing both upstream and downstream tasks are executed to scrutinize the influence of inductive bias on deep model learning. Our findings underscore the following key points: (i) the contribution of network engineering design is paramount to achieving performance gains, emphasizing the importance of thoughtful architecture choices; (ii) certain STMs, even those considered relatively early, can attain state-of-the-art performance when coupled with modern design principles.

This work endeavors to serve as a well-optimized platform for the development of new vision backbones, particularly those integrating advanced spatial feature aggregation mechanisms. The downstream task results and nuanced analyses yield valuable insights for practitioners, aiding them in the judicious selection of suitable backbones for their specific applications. While our study offers comprehensive insights, we acknowledge certain limitations and outline directions for future research. Our forthcoming work will focus on evaluating STMs within larger models and diverse datasets to bolster generalizability and robustness. Additionally, we plan to broaden the evaluation scope, encompassing a diverse range of downstream tasks, to provide a more thorough understanding of STM performance across various applications.

REFERENCES

- [1] A. Dosovitskiy, L. Beyer, A. Kolesnikov, D. Weissenborn, X. Zhai, T. Unterthiner, M. Dehghani, M. Minderer, G. Heigold, S. Gelly *et al.*, “An image is worth 16x16 words: Transformers for image recognition at scale,” *arXiv preprint arXiv:2010.11929*, 2020. **1, 3, 5**
- [2] A. Vaswani, P. Ramachandran, A. Srinivas, N. Parmar, B. Hechtman, and J. Shlens, “Scaling local self-attention for parameter efficient visual backbones,” in *CVPR*, 2021, pp. 12 894–12 904. **1, 2, 3, 4, 6**
- [3] Z. Liu, Y. Lin, Y. Cao, H. Hu, Y. Wei, Z. Zhang, S. Lin, and B. Guo, “Swin transformer: Hierarchical vision transformer using shifted windows,” in *ICCV*, 2021, pp. 10 012–10 022. **1, 2, 3, 4, 5, 6**
- [4] W. Wang, E. Xie, X. Li, D.-P. Fan, K. Song, D. Liang, T. Lu, P. Luo, and L. Shao, “Pyramid vision transformer: A versatile backbone for dense prediction without convolutions,” in *ICCV*, 2021, pp. 568–578. **1, 2, 3, 4**
- [5] Z. Liu, H. Mao, C.-Y. Wu, C. Feichtenhofer, T. Darrell, and S. Xie, “A convnet for the 2020s,” in *CVPR*, 2022, pp. 11 976–11 986. **1, 2, 3, 4, 5, 6**
- [6] X. Ding, X. Zhang, J. Han, and G. Ding, “Scaling up your kernels to 31x31: Revisiting large kernel design in cnns,” in *CVPR*, 2022, pp. 11 963–11 975. **1, 3, 4, 8**
- [7] S. Liu, T. Chen, X. Chen, X. Chen, Q. Xiao, B. Wu, M. Pechenizkiy, D. Mocanu, and Z. Wang, “More convnets in the 2020s: Scaling up kernels beyond 51x51 using sparsity,” *arXiv preprint arXiv:2207.03620*, 2022. **1, 3**
- [8] Z. Dai, H. Liu, Q. V. Le, and M. Tan, “CoAtNet: Marrying convolution and attention for all data sizes,” *NeurIPS*, vol. 34, pp. 3965–3977, 2021. **1**
- [9] Y. Rao, W. Zhao, Y. Tang, J. Zhou, S.-N. Lim, and J. Lu, “Hornet: Efficient high-order spatial interactions with recursive gated convolutions,” *arXiv preprint arXiv:2207.14284*, 2022. **1**
- [10] W. Yu, M. Luo, P. Zhou, C. Si, Y. Zhou, X. Wang, J. Feng, and S. Yan, “Metaformer is actually what you need for vision,” in *CVPR*, 2022, pp. 10 809–10 819. **1, 3, 4, 5**

- [11] H. Touvron, M. Cord, M. Douze, F. Massa, A. Sablayrolles, and H. Jegou, "Training data-efficient image transformers & distillation through attention," in *ICML*, ser. Proceedings of Machine Learning Research, M. Meila and T. Zhang, Eds., vol. 139, 18–24 Jul 2021, pp. 10347–10357. [Online]. Available: <https://proceedings.mlr.press/v139/touvron21a.html> 1
- [12] A. Vaswani, N. Shazeer, N. Parmar, J. Uszkoreit, L. Jones, A. N. Gomez, Ł. Kaiser, and I. Polosukhin, "Attention is all you need," *NeurIPS*, vol. 30, 2017. 2, 4, 5
- [13] X. Dong, J. Bao, D. Chen, W. Zhang, N. Yu, L. Yuan, D. Chen, and B. Guo, "Cswin transformer: A general vision transformer backbone with cross-shaped windows," in *CVPR*, 2022, pp. 12124–12134. 1, 4
- [14] W. Wang, J. Dai, Z. Chen, Z. Huang, Z. Li, X. Zhu, X. Hu, T. Lu, L. Lu, H. Li *et al.*, "InternImage: Exploring large-scale vision foundation models with deformable convolutions," in *CVPR*, 2023. 2, 3, 4, 6
- [15] J. Deng, W. Dong, R. Socher, L.-J. Li, K. Li, and L. Fei-Fei, "Imagenet: A large-scale hierarchical image database," in *CVPR*, 2009, pp. 248–255. 2, 5
- [16] T.-Y. Lin, M. Maire, S. Belongie, J. Hays, P. Perona, D. Ramanan, P. Dollár, and C. L. Zitnick, "Microsoft coco: Common objects in context," in *ECCV*, 2014, pp. 740–755. 2
- [17] W. Luo, Y. Li, R. Urtasun, and R. Zemel, "Understanding the effective receptive field in deep convolutional neural networks," *NeurIPS*, vol. 29, 2016. 2, 8
- [18] W. Wang, E. Xie, X. Li, D.-P. Fan, K. Song, D. Liang, T. Lu, P. Luo, and L. Shao, "Pvt v2: Improved baselines with pyramid vision transformer," *Computational Visual Media*, vol. 8, no. 3, pp. 415–424, 2022. 3
- [19] Q. Han, Z. Fan, Q. Dai, L. Sun, M.-M. Cheng, J. Liu, and J. Wang, "On the connection between local attention and dynamic depth-wise convolution," in *ICLR*, 2021. 3, 4
- [20] I. Goodfellow, Y. Bengio, and A. Courville, *Deep Learning*, 2016, <http://www.deeplearningbook.org>. 3, 8
- [21] A. Krizhevsky, I. Sutskever, and G. E. Hinton, "Imagenet classification with deep convolutional neural networks," *Communications of the ACM*, vol. 60, no. 6, pp. 84–90, 2017. 3
- [22] K. Simonyan and A. Zisserman, "Very deep convolutional networks for large-scale image recognition," *arXiv preprint arXiv:1409.1556*, 2014. 3
- [23] C. Szegedy, W. Liu, Y. Jia, P. Sermanet, S. Reed, D. Anguelov, D. Erhan, V. Vanhoucke, and A. Rabinovich, "Going deeper with convolutions," in *CVPR*, 2015, pp. 1–9. 3
- [24] K. He, X. Zhang, S. Ren, and J. Sun, "Deep residual learning for image recognition," in *CVPR*, 2016, pp. 770–778. 3, 5
- [25] G. Huang, Z. Liu, L. Van Der Maaten, and K. Q. Weinberger, "Densely connected convolutional networks," in *CVPR*, 2017, pp. 4700–4708. 3
- [26] A. G. Howard, M. Zhu, B. Chen, D. Kalenichenko, W. Wang, T. Weyand, M. Andreetto, and H. Adam, "Mobilenets: Efficient convolutional neural networks for mobile vision applications," *arXiv preprint arXiv:1704.04861*, 2017. 3
- [27] S. Xie, R. Girshick, P. Dollár, Z. Tu, and K. He, "Aggregated residual transformations for deep neural networks," in *CVPR*, 2017, pp. 1492–1500. 3
- [28] J. Hu, L. Shen, and G. Sun, "Squeeze-and-excitation networks," in *CVPR*, 2018, pp. 7132–7141. 3
- [29] J. Dai, H. Qi, Y. Xiong, Y. Li, G. Zhang, H. Hu, and Y. Wei, "Deformable convolutional networks," in *ICCV*, 2017, pp. 764–773. 3, 4
- [30] X. Wang, R. Girshick, A. Gupta, and K. He, "Non-local neural networks," in *CVPR*, 2018, pp. 7794–7803. 3
- [31] S. Wang, B. Z. Li, M. Khabsa, H. Fang, and H. Ma, "Linformer: Self-attention with linear complexity," *arXiv preprint arXiv:2006.04768*, 2020. 3
- [32] S. Wu, T. Wu, H. Tan, and G. Guo, "Pale transformer: A general vision transformer backbone with pale-shaped attention," in *AAAI*, vol. 36, no. 3, 2022, pp. 2731–2739. 3, 4
- [33] R. Wightman, H. Touvron, and H. Jégou, "Resnet strikes back: An improved training procedure in timm," *arXiv preprint arXiv:2110.00476*, 2021. 3
- [34] W. Yu, C. Si, P. Zhou, M. Luo, Y. Zhou, J. Feng, S. Yan, and X. Wang, "Metaformer baselines for vision," *arXiv preprint arXiv:2210.13452*, 2022. 3
- [35] R. Wightman, "Pytorch image models," <https://github.com/rwightman/pytorch-image-models>, 2019. 3
- [36] X. Zhu, H. Hu, S. Lin, and J. Dai, "Deformable convnets v2: More deformable, better results," in *CVPR*, 2019, pp. 9308–9316. 4
- [37] I. Loshchilov and F. Hutter, "Decoupled weight decay regularization," *arXiv preprint arXiv:1711.05101*, 2017. 5
- [38] H. Touvron, M. Cord, A. Sablayrolles, G. Synnaeve, and H. Jégou, "Going deeper with image transformers," in *ICCV*, 2021, pp. 32–42. 5
- [39] C. Szegedy, V. Vanhoucke, S. Ioffe, J. Shlens, and Z. Wojna, "Rethinking the inception architecture for computer vision," in *CVPR*, 2016, pp. 2818–2826. 5
- [40] G. Huang, Y. Sun, Z. Liu, D. Sedra, and K. Q. Weinberger, "Deep networks with stochastic depth," in *ECCV*. Springer, 2016, pp. 646–661. 5
- [41] E. D. Cubuk, B. Zoph, J. Shlens, and Q. V. Le, "RandAugment: Practical automated data augmentation with a reduced search space," in *CVPR*, 2020, pp. 702–703. 5
- [42] H. Zhang, M. Cisse, Y. N. Dauphin, and D. Lopez-Paz, "mixup: Beyond empirical risk minimization," *arXiv preprint arXiv:1710.09412*, 2017. 5
- [43] S. Yun, D. Han, S. J. Oh, S. Chun, J. Choe, and Y. Yoo, "Cutmix: Regularization strategy to train strong classifiers with localizable features," in *ICCV*, 2019, pp. 6023–6032. 5
- [44] Z. Zhong, L. Zheng, G. Kang, S. Li, and Y. Yang, "Random erasing data augmentation," in *AAAI*, vol. 34, no. 07, 2020, pp. 13001–13008. 5
- [45] K. He, G. Gkioxari, P. Dollár, and R. Girshick, "Mask R-CNN," in *ICCV*, 2017, pp. 2961–2969. 5
- [46] Z. Liu, H. Hu, Y. Lin, Z. Yao, Z. Xie, Y. Wei, J. Ning, Y. Cao, Z. Zhang, L. Dong *et al.*, "Swin transformer v2: Scaling up capacity and resolution," in *CVPR*, 2022, pp. 12009–12019. 6
- [47] R. Zhang, "Making convolutional networks shift-invariant again," in *ICML*, 2019, pp. 7324–7334. 8